

# *In situ* X-ray diffraction study on the growth kinetics of NiO nanoparticles

C. T. Meneses,<sup>a\*</sup> J. M. A. Almeida<sup>a</sup> and J. M. Sasaki<sup>b</sup>

Received 29 September 2009

Accepted 15 March 2010

<sup>a</sup>Núcleo de Física, Universidade Federal de Sergipe, Campus Professor Alberto Carvalho, 49500-000 Itabaiana, SE, Brazil, and <sup>b</sup>Departamento de Física, Universidade Federal do Ceará, Campus do Pici, CP 6030, 60455-760 Fortaleza, CE, Brazil. E-mail: cmeneses@fisica.ufs.br

The growth kinetics of NiO nanoparticles have been studied by *in situ* X-ray diffraction using two detection systems (conventional and imaging plate). NiO nanoparticles were formed by thermal decomposition after heating of an amorphous compound formed by the coprecipitation method. It was found that the detection method using an imaging plate is more efficient than the conventional detection mode for observing changes in the crystallite growth of nanocrystalline materials. Studies have been carried out to investigate the effects of the heating rates on the particles growth. The results suggest that the growth process of the particles is accelerated when the samples are treated at low heating rates. The evolution of particles size and the diffusion coefficient obtained from X-ray powder diffraction patterns are discussed in terms of the thermal conditions for the two types of detection.

© 2010 International Union of Crystallography  
Printed in Singapore – all rights reserved

**Keywords:** X-ray diffraction; nanoparticles; imaging plate.

## 1. Introduction

In recent years studies involving *in situ* X-ray diffraction using synchrotron radiation have increased tremendously and have proved to be milestones in studies of time-resolved crystallization and structural changes in several materials (Zolliker *et al.*, 1990; Danzig *et al.*, 1995; Morris *et al.*, 1996; Svensson *et al.*, 1997; Liang *et al.*, 2003; Natter *et al.*, 2000; Beale & Sankar, 2003). Although some studies use *in situ* X-ray diffraction (Danzig *et al.*, 1995; Gualtieri *et al.*, 1996; Natter *et al.*, 2000) or small-angle X-ray scattering techniques (Vleeshouwers, 1997; Kranold *et al.*, 2003) to study the kinetics of growth, crystallization and particle nucleation, such studies are conducted using only one detection system. Certainly, interest in these studies is of fundamental importance for controlling the synthesis and determining particle size and distribution as desired. Good control of these parameters is the main reason for these materials to be used for future applications (Jana *et al.*, 2004).

In our previous work (Meneses *et al.*, 2007a) we emphasized theoretical and experimental studies using X-ray absorption near-edge spectroscopy (XANES) to investigate the crystallization process of NiO nanoparticles. In this study we verified the amorphous–crystalline transitions and determined the initial temperature of the growth process of the nanoparticles. However, in the particular case of NiO nanoparticles, it was not possible to obtain *via* XANES spectra quantitative information on the particle growth or check nucleation rates for the growth of these particles. In this paper we have studied the crystallization process in order to obtain quantitative infor-

mation on the growth of NiO nanoparticles through analysis of *in situ* X-ray powder diffraction (XRPD) using synchrotron radiation by two detection systems: a conventional detector for the  $\theta$ – $2\theta$  linear mode, and an imaging plate using the scattering-reflection mode. The results were also analyzed for two different heating rates to study the growth rates of the particles at different temperatures.

## 2. Experimental

All experiments were performed using the six-circle diffractometer (Huber) with  $\theta$ – $2\theta$  analyzer on beamline D10B-XPD at the Brazilian Synchrotron Light Laboratory (LNLS), Campinas, Brazil (Ferreira *et al.*, 2006). For such experiments two sets of 1.3 mm slits were used, both located between the input and output beam in the sample. The beamline has a focused optical beam with a pre-mirror, a double-crystal Si monochromator and a cylindrical mirror focus. The wavelength used in the experiments was 1.4938 (5) Å. A schematic view of the imaging-plate system is shown in Fig. 1. Measurements obtained using the imaging-plate detector were collected in the scattering-reflection mode using a beam exposure time of 2 min. The diffracted data were collected in the  $2\theta$  range 20–70°. Therefore we only use the two most intense peaks of cubic NiO. The data were collected on a Fuji flat (20 × 40 cm) and scanned using an XXX scanner. The imaging plate was mounted perpendicular to the incoming beam at a distance of ~20 cm from the sample (Fig. 1). The conversion from pixels to angle  $2\theta$  was carried out using parameters determined from Rietveld refinement of Al<sub>2</sub>O<sub>3</sub>

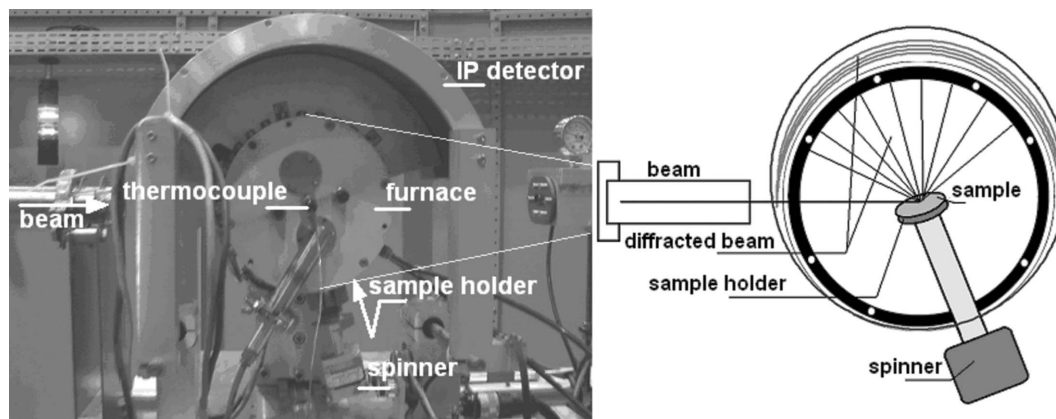


**Figure 1**  
Photograph and schematic view of the experimental set-up of the imaging-plate detector and components.

(SRM 676) standard sample peak positions. The full width at half-maximum for each peak of the sample was corrected for instrumental broadening for the two systems using a standard sample of  $\text{Al}_2\text{O}_3$  (size  $\sim 10\ \mu\text{m}$ ). For the other experiments a Cyberstar scintillator detector was used, continuously scanning in  $2\theta$  from  $39$  to  $45^\circ$  in steps of  $0.01^\circ$  at an angular speed of  $0.01\ \text{s}^{-1}$  to obtain the most intense peak of NiO {002}.

In all experiments fine powders of the precursor material of composition NiO/NaCl (amorphous/crystalline), prepared as described by Meneses *et al.* (2007b) and pre-treated at  $573\ \text{K}$  for  $30\ \text{min}$ , were synthesized (the NaCl was used to correct the angular positions of the peaks).  $150\ \text{mg}$  of the material was pressed into pellets [ $10\ \text{mm} \times 3\ \text{mm}$  (diameter  $\times$  thickness)] and placed in a ceramic sample holder, which was rotated at constant speed. The sample holder was placed in a circular furnace at ambient atmosphere and positioned at a distance of  $3\ \text{mm}$  from a temperature sensor, a type-K thermocouple. In both experiment types (imaging plate and conventional) we used two heating rates,  $5$  and  $10\ \text{K min}^{-1}$ , up to  $773\ \text{K}$  and diffraction patterns were collected in steps each of  $15\ \text{K}$  starting from  $623\ \text{K}$ , waiting for  $1\ \text{min}$  to stabilize at each measurement. This temperature was chosen according to the thermal analysis of the crystallization process found in XANES measurements (Meneses *et al.*, 2007c) and the preliminary results of thermogravimetric analysis reported by Maia *et al.* (2005), where the first crystallization stage was observed. Diffraction patterns were collected for both systems after thermal equilibrium was reached, *i.e.* after about  $1\ \text{min}$ . For the experiments using the imaging-plate detector, the sample in the sample holder was placed in the furnace and the furnace kept at an angle of  $16.7^\circ$  relative to the incident beam, as shown in Fig. 1(b).

### 3. Results and discussion

All results and analysis presented here show the kinetics of the formation and growth of NiO nanoparticles through *in situ* XRPD studies for two heating rates,  $5$  and  $10\ \text{K min}^{-1}$ . Fig. 2 shows X-ray diffraction (XRD) patterns obtained from conventional  $\theta$ - $2\theta$  measurements. These results show only the

evolution of the reflection {002} of the face-centred-cubic NiO and a peak corresponding to the reflection {220} of NaCl. At  $593\ \text{K}$  the structure is crystalline-like, indicating the initial stage of formation of NiO nanoparticles. These results show that the onset of crystallization and growth of NiO particles takes place at  $693\ \text{K}$ . Regardless of the heating rates, it is evident from the inset of Fig. 2(a) that the intensity of the

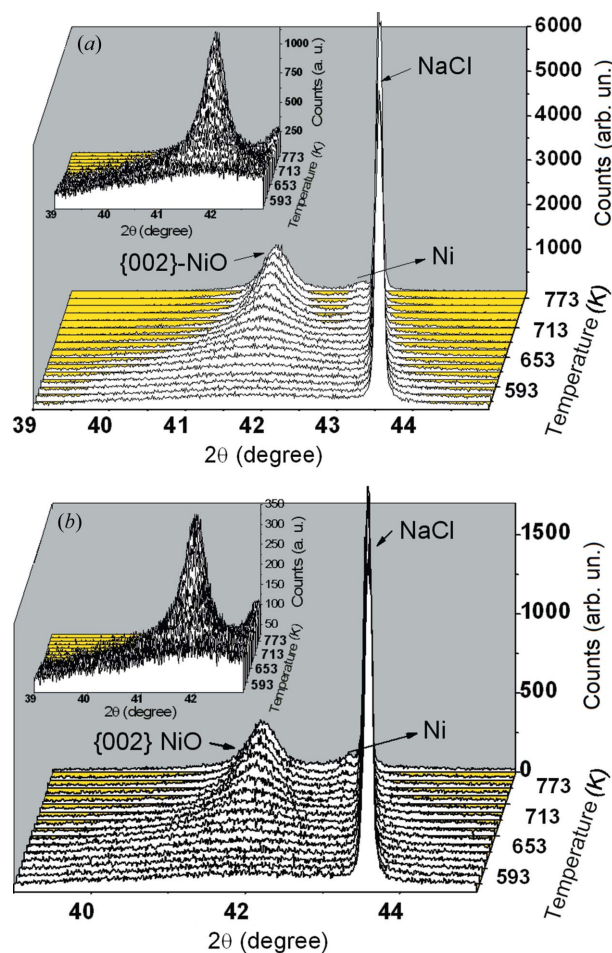


**Figure 2**  
X-ray diffraction patterns collected using the conventional detector, obtained at heating rates of (a)  $5\ \text{K min}^{-1}$  and (b)  $10\ \text{K min}^{-1}$ .

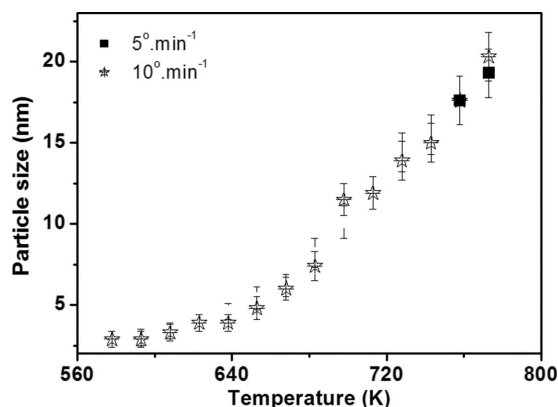


**Figure 3** Calculated particle size as a function of temperature obtained using the conventional detector.

reflections of NiO increases with increasing temperature, which is attributed to the gradual increase in the number and size of particles, and particularly the improvement of crystallinity of the nanoparticles. These results show also that there is not dependence on heating rates in the particle growth. Fig. 3 shows clearly that no difference is observed for the samples treated with heating rates of 5 and 10 K min<sup>-1</sup>. Moreover, it was found that the systems show two stages in the particle growth (before and after 673 K). The first stage can be attributed mainly to the nucleation process up to 673 K, indicating that the particles are amorphous. After this temperature, particle growth is fast, which is attributed to crystallization of the particles (grain growth). Differences in the two sets of samples were not detected, probably due to the acquisition time of the XRD pattern, which is relatively high compared with the growth rate of the particles.

To confirm our assumptions and determine the best conditions for nucleation and growth of the particles, we used an imaging-plate detection system. In this experiment it is possible to identify differences in the growth of the particles as a function of heating rate as compared to the results obtained by a conventional detection mode. Fig. 4 shows the XRD patterns of the reflections {002} and {111} of NiO as a function of the temperature and heating rate. One can conclude that this set of results yields a better way to observe the growth of particles by means of peak profiles. We note a clear increase in the intensity from 698 K and 728 K for the samples treated at 5 K min<sup>-1</sup> and 10 K min<sup>-1</sup>, respectively. This result indicates the beginning of crystallization and growth according to the results obtained by the conventional system. However, it is worth noticing that the initial stage of crystallization and the differences between heating rates can be better observed using the imaging plates (see Figs. 3 and 5). It has been shown previously (Meneses *et al.*, 2007a) through XAS experiment that this may be related to the nucleation time. Furthermore, we have observed that increasing heating rates decrease the growth rate of the particles. On the other hand, there is a compromise between the heating rates and the degree of disorder of the samples: the lower the heating rates the greater the degree of disorder (Meneses *et al.*, 2007c). A higher degree

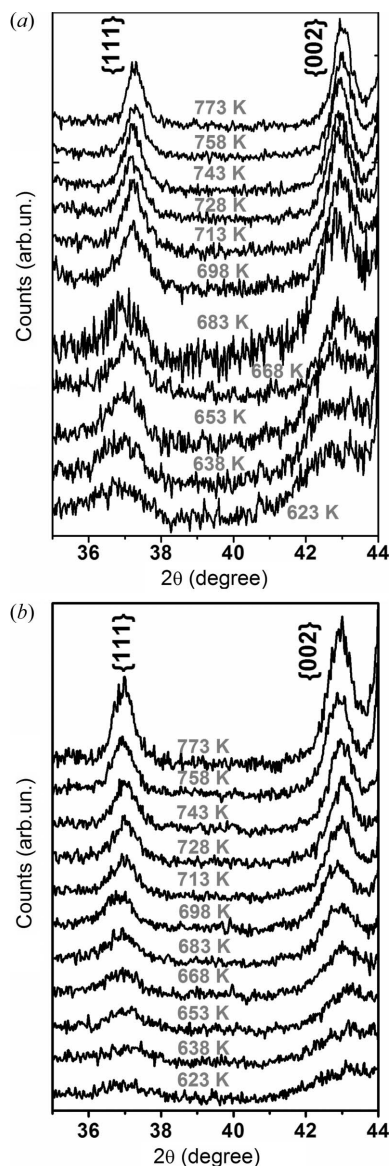


**Figure 4** X-ray diffraction patterns collected using the imaging-plate detector, obtained at heating rates of (a) 5 K min<sup>-1</sup> and (b) 10 K min<sup>-1</sup>.

of disorder can lead to stacking faults or dislocations of the planar lattice, increasing the effect of strain.

By using equation (1), as described by Danzig *et al.* (1995),

$$D(t, T) = D_0(T)[(t - t_0)]^{1/2}, \quad (1)$$

where  $D$  is the mean particle size estimated by Scherrer's equation,  $t$  is the time,  $T$  is the temperature and  $D_0$  is the diffusion coefficient, the mean diffusion coefficients of reflections {111} and {002} for all XRD experiments were determined from measurement as a function of time at 593 K for 60 min. This temperature was fixed for all systems because the diffusion coefficient increases with temperature (Danzig *et al.*, 1995). It was chosen as it determines the first stage of crystallization of the particles. This coefficient is an important parameter for controlling the particles' growth. The increase of this coefficient can lead to the system having a larger

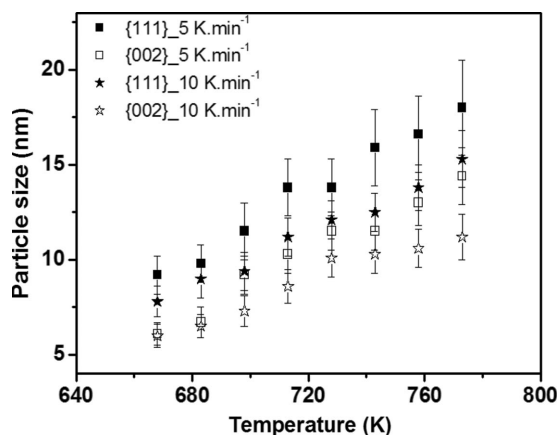


**Figure 5**  
Calculated particle size as a function of temperature obtained using the imaging-plate detector for crystallographic plane families {111} and {002}.

particles sizes distribution. We do not observe differences in the diffusion coefficient with the use of a conventional detection system (see Table 1). Moreover, the experimental data obtained from use of the imaging-plate detector show a decrease in dispersion coefficient with increasing heating rate. These results indicate that the heating rate influences the particle size. However, we are only able to detect this using the very sensitive imaging-plate technique.

#### 4. Conclusion

To summarize, we have studied the growth and formation of NiO nanoparticles through *in situ* XRPD studies using two detection systems and an amorphous precursor made of salt and an organic agent. The results demonstrate the potential of time-resolved *in situ* XRPD using an imaging-plate detector to study the kinetics of formation and controlled growth of nanoparticles. The results also show that the heating rate used in the synthesis process is an important feature for controlling particle size. It was found that low heating rates accelerate growth of the particles.

The authors are grateful for access to the facilities at the X-ray powder diffraction beamline at the LNLS under proposal D10B-XPD-4631. We thank Dr Surender Kumar

**Table 1**

Diffusion coefficients obtained for different heating rates and different detection systems.

Imaging-plate detector		Conventional detector	
Rate (K min <sup>-1</sup> )	$D_0$ (Å <sup>2</sup> s <sup>-1</sup> )	Rate (K min <sup>-1</sup> )	$D_0$ (Å <sup>2</sup> s <sup>-1</sup> )
5 {111}	1.9 (2)	5	2.4 (3)
5 {002}	1.3 (1)	10	2.4 (3)
10 {111}	1.3 (1)		
10 {002}	0.9 (1)		

Sharma for suggestions and a critical reading of the manuscript. This work has also been funded by the Brazilian agency CNPq.

#### References

- Beale, A. M. & Sankar, G. (2003). *Chem. Mater.* **15**, 146–153.
- Danzig, A., Mattern, N. & Doyle, S. (1995). *Nucl. Instrum. Methods Phys. Res. B*, **97**, 465–467.
- Ferreira, F. F., Granado, E., Carvalho Jr, W., Kycia, S. W., Bruno, D. & Droppa Jr, R. (2006). *J. Synchrotron Rad.* **13**, 46–53.
- Gualtieri, A., Norby, P., Hanson, J. & Hriljac, J. (1996). *J. Appl. Cryst.* **29**, 707–713.
- Jana, N. R., Chen, Y. F. & Peng, X. G. (2004). *Chem. Mater.* **16**, 3931–3935.
- Kranold, R., Kriesen, S., Haselhoff, M., Weber, H.-J. & Goerigk, G. (2003). *J. Appl. Cryst.* **36**, 410–414.
- Liang, J. Y., Lin, G., Bin, X. H., Jing, L., Dong, L. X., Hua, W. Z., Yu, W. Z. & Weber, J. (2003). *J. Cryst. Growth*, **252**, 226–229.
- Maia, A. O. G., Meneses, C. T., Menezes, A. S., Melo, D. M. & Sasaki, J. M. (2005). *J. Non-Cryst. Solids*, **352**, 3729.
- Menezes, C. T., Flores, W. H., Garcia, F. & Sasaki, J. M. (2007b). *J. Nanopart. Res.* **9**, 501–505.
- Menezes, C. T., Flores, W. H. & Sasaki, J. M. (2007a). *Chem. Mater.* **19**, 1024–1027.
- Menezes, C. T., Flores, W. H. & Sasaki, J. M. (2007c). *J. Electron Spectrosc. Relat. Phenom.* **156–158**, 176–179.
- Morris, R. E., Weigel, S. J., Norby, P., Hanson, J. C. & Cheetham, A. K. (1996). *J. Synchrotron Rad.* **3**, 301–304.
- Natter, H., Schmelzer, M., Löffler, M.-S., Krill, C. E., Fitch, A. & Hempelmann, R. (2000). *J. Phys. Chem. B*, **104**, 2467–2476.
- Svensson, S. O., Birch, J., Müller, H. & Kvik, Å. (1997). *J. Synchrotron Rad.* **4**, 83–94.
- Vleeshouwers, S. (1997). *Polymer*, **38**, 3213–3221.
- Zolliker, P., Cox, D. E., Parize, J. B., McCarron, E. M. & Farneth, W. E. (1990). *Phys. Rev. B*, **42**, 6332–6341.